9

LENS ANTENNAS

In lenses, as in parabolic reflectors, we utilize free space as a feed network to excite a large aperture. Because we locate the feed behind the aperture, the configuration eliminates aperture blockage and allows direct connection of the feed to the transmitter or receiver. When frequencies are above microwaves, this feeding method removes lossy transmission lines that increase system noise.

Lenses have only half the tolerance requirements of reflectors because the wave passes by the anomaly only once. In a reflector the wave path deviates by twice the distance as the wave travels to and from the reflector. At low microwave frequencies the lens is prohibitively heavy, but zoning and the use of artificial dielectrics reduce this problem. Both zoning and artificial dielectrics present mechanical stability problems and narrow the bandwidth.

We organize the design of lenses by the available degrees of freedom. A single lens with a uniform dielectric has two surfaces and is equivalent to a dual reflector because each surface is a degree of freedom. We start our discussion with single-surface lenses where we eliminate one degree of freedom by making the second surface match either the incoming or outgoing wave. Shaping both surfaces lets us correct one lens anomaly. We can remove either coma to improve the feed scanning or design to convert a given feed pattern to a desired aperture distribution. Bootlace lenses have three possible degrees of freedom. They consist of back-to-back arrays with cables connecting the sides. Normally, we use the degrees of freedom of the bootlace lens to increase the number of focal points. We give up degrees of freedom in many designs to simplify the mechanical layout. Finally, we discuss the use of a variable index of refraction in the Luneburg lens.

We base the design of lenses on geometric optics. Like parabolic reflectors, lenses have no inherent frequency bandwidth limitation. We are limited by the feeds and mechanical problems of large sizes. Because we borrow from optics, lenses have great high-frequency potential.

Modern Antenna Design, Second Edition, By Thomas A. Milligan

9-1 SINGLE REFRACTING SURFACE LENSES

Single-surface lenses convert the wave type, such as spherical to planar, at one surface through refraction. The constant-phase surface (eikonal) of the wave type determines the shape of the second surface of the lens. The common lens converts an incident spherical or cylindrical wave to a plane wave. Conversion to a cylindrical wave requires a line source feed and cylindrical surfaces on the lens. Spherical waves use point feeds and axisymmetrical surfaces. Like the reflector, which also converts spherical waves from the feed to plane waves by geometric optics (GO), diffraction from an aperture determines the far-field pattern.

Consider the second or nonrefracting surface. If the surface toward the feed converts the wave type, the wave exits the second surface as a plane wave and it is a plane. Similarly, when the surface away from the feed converts the exiting wave to a plane wave, the inner surface toward the feed follows the incident wave eikonal, a cylindrical or spherical surface. Figure 9-1 shows the two types of single refracting surface lenses. We can determine the refracting surface shape by either of two different approaches. Snell's law can be applied to the refracting surface, and the surface slope can be determined for each feed angle. Equivalently, we can apply Fermat's principle to equalize the optical path length from the feed through the lens to an aperture plane. The designs are easily found [1,2]. For Figure 9-1*a*,

$$\rho(\psi) = \frac{(n-1)f}{n\cos\psi - 1} \tag{9-1}$$

where n is the index of refraction, given by

$$n = \sqrt{\varepsilon_r \mu_r} \tag{9-2}$$

and ε_r and μ_r are the relative permittivity and permeability of the lens medium. When $n > 1$, Eq. (9-1) describes a hyperbola with the feed at one focus. The distance from the feed to the hyperbola along the axis is f. The asymptotes of the hyperbola limit the collimated portion of the feed radiation:

$$\psi_a = \cos^{-1}\frac{1}{n} \tag{9-3}$$

We must limit the lens edge to angles less than ψ_a because the asymptotes imply an infinite aperture size. Similar to the paraboloidal reflector, we have feed spillover, considered to be lost in sidelobes. But, for example, placing the lens at the aperture of a horn eliminates spillover. We calculate the lens diameter from

$$D = 2\rho\sin\psi_e = \frac{2(n-1)f\sin\psi_e}{n\cos\psi_e - 1} \tag{9-4}$$

where ψ_e is the edge angle, subject to the restriction of Eq. (9-3). The surfaces of the lens in Figure 9-l*b* have the polar equations

$$\rho_1 = \text{constant} \qquad \rho_2(\psi) = \frac{(n-1)f}{n - \cos\psi} \tag{9-5}$$

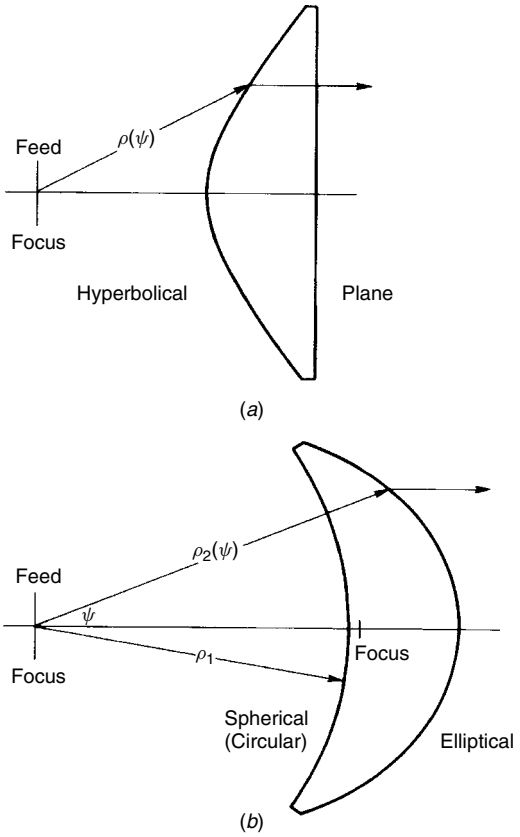

FIGURE 9-1 Single-surface lenses.

The inner surface must either be a circular cylinder (cylindrical lens) or be spherical (axisymmetrical lens). The outer surface $\rho_2(\psi)$ is elliptical for $n > 1$. The junction of the circle and ellipse determines the feed angle limitation:

$$\cos \psi_e = n - \frac{(n-1)f}{\rho_1} \tag{9-6}$$

We can, of course, truncate the lens before the two curves meet. Equation (9-6) gives the limitation on ρ_1 at the lens edge as well:

$$\rho_1 \leq \frac{(n-1)f}{n - \cos \psi_e} \tag{9-7}$$

Example Compute f and ρ_1 at the edge for an elliptical lens (Figure 9-l*b*) with $D = 10\lambda$, $n = 1.6$ (polystyrene), and $\psi_e = 50^\circ$.

Solve Eq. (9-5) for f/D:

$$\frac{f}{D} = \frac{n - \cos \psi_e}{2 \sin \psi_e (n-1)} \qquad f = 10.41\lambda \tag{9-8}$$

$$\rho_1 \leq \frac{D}{2 \sin \psi_e} \tag{9-9}$$

If ρ_1 remained constant to the center of the lens, it would be 3.88λ thick. In narrowband applications we can remove the multiple wavelength thicknesses by zoning and reduce weight and dielectric material loss.

Lenses change the amplitude distribution of the feed in the aperture plane. We relate the feed pattern to the aperture distribution through the conservation of power in differential areas. For an axisymmetrical lens:

$$\underset{\text{feed power}}{F(\psi, \phi) \sin \psi \, d\psi \, d\phi} = \underset{\text{aperture power}}{A(r, \phi) r \, dr \, d\phi} \tag{9-10}$$

where ψ is the feed angle and r, $\rho \sin \psi$, is the aperture radial distance; $F(\psi, \phi)$ is the feed power pattern and $A(r, \phi)$ is the aperture power distribution:

$$\frac{A(r, \phi)}{F(\psi, \phi)} = \frac{\sin \psi}{r} \frac{d\psi}{dr} \tag{9-11}$$

For a cylindrical lens, we also equate differential area multiplied by the feed or aperture power:

$$\begin{aligned} F(\psi, y) \, d\psi \, dy &= A(r, y) \, dr \, dy \\ \frac{A(r, y)}{F(\psi, \phi)} &= \frac{d\psi}{dr} \end{aligned} \tag{9-12}$$

We substitute Eqs. (9-11) and (9-12) into Eq. (9-1) for the hyperbolical lens to calculate the aperture distribution relative to the feed power pattern.

$$\underset{\text{Axisymmetrical}}{\frac{A(r, \phi)}{F(\psi, \phi)} = \frac{(n \cos \psi - 1)^3}{f^2 (n-1)^2 (n - \cos \psi)}} \qquad \underset{\text{Cylindrical}}{\frac{A(r, y)}{F(\psi, y)} = \frac{(n \cos \psi - 1)^2}{f (n-1)(n - \cos \psi)}} \tag{9-13a, b}$$

The field distribution is the square root of Eq. (9-13).

We substitute Eqs. (9-11) and (9-12) into Eq. (9-5) for the elliptical lens:

$$\underset{\text{Axisymmetrical}}{\frac{A(r, \phi)}{F(\psi, \phi)} = \frac{(n - \cos \psi)^3}{f^2 (n-1)(n \cos \psi - 1)}} \qquad \underset{\text{Cylindrical}}{\frac{A(r, y)}{F(\psi, \phi)} = \frac{(n - \cos \psi)^2}{f (n-1)(n \cos \psi - 1)}} \tag{9-14a, b}$$

The hyperbolical and elliptical lenses concentrate the aperture power in different ways. The hyperbolical lens reduces the feed power directed toward the edges and produces an additional aperture taper. On the other hand, an elliptical single-surface lens increases the power toward the edges as compared with the center.

Example For axisymmetrical lenses with $\psi_e = 50^\circ$ and $n = 1.6$, compute the edge taper due to the lenses.

We divide Eq. (9-13*b*) with $\psi_e = \psi$ by the same equation with $\psi = 0$ to determine the ratio of power at the edge to that at the center of the aperture (assuming an isotropic feed). We do the same calculation with Eq. (9-14*a*):

$$\frac{A_e}{A_c} = \begin{cases} \dfrac{(n\cos\psi_e - 1)^3}{(n-1)^2(n-\cos\psi_e)} & \text{hyperbolical lens} \quad (9\text{-}15) \\ \dfrac{(n-\cos\psi_e)^3}{(n-1)^2(n\cos\psi_e - 1)} & \text{elliptical lens} \quad (9\text{-}16) \end{cases}$$

By substituting ψ_e and n, we compute the edge taper.

hyperbolical lens: 0.038 (−14.2 dB) elliptical lens : 7.14 (8.5 dB)

The increased taper of the hyperbolical lens reduces sidelobes, and the elliptical lens increases aperture efficiency by compensating for some of the feed antenna pattern taper to make the aperture distribution more uniform.

9-2 ZONED LENSES

Lenses designed by the methods of Section 9-1 have bandwidth limitations determined only by the invariability of the dielectric constant. Zoning removes multiples-of-wavelength path lengths in the lens to reduce weight, to reduce the lens-induced amplitude taper, or to thin the lens. The act of changing dimensions by wavelengths implies narrowing the frequency bandwidth.

We step the lens in either the nonrefracting or refracting surface. Stepping the nonrefracting surface (Figure 9-2*a, b*) has the least effect. The edges of the steps, parallel with the waves, will diffract waves and cause some change in the aperture fields, but GO predicts no effect. Stepping the refracting surface introduces losses either as misdirected feed power (Figure 9-2*c, d*) or as unexcited aperture (Figure 9-2*e, f*). But stepping the refracting surface reduces the lens-induced aperture taper by changing the focal lengths in various zones. Figure 9-2 shows the limits in the two types of refracting surface steps, since we could compromise between the directions and have both feed spillover and unexcited aperture.

We can easily calculate the step dimensions in Figure 9.2*a* and *b*. We equate the path lengths inside and outside the dielectric along the step with a difference of Δ or some integer multiple of λ:

$$\underset{\text{inside}}{n\Delta} = \underset{\text{outside}}{\Delta + \lambda}$$

The step Δ becomes

$$\Delta = \frac{\lambda}{n-1} \tag{9-17}$$

In Figure 9-2*c–f* we determine the change in focal lengths instead of the step dimensions. Zoning affects the optical path lengths in the center of the lens. We calculate the edge focal length from the unzoned case. The focal length increases by Eq. (9-17)

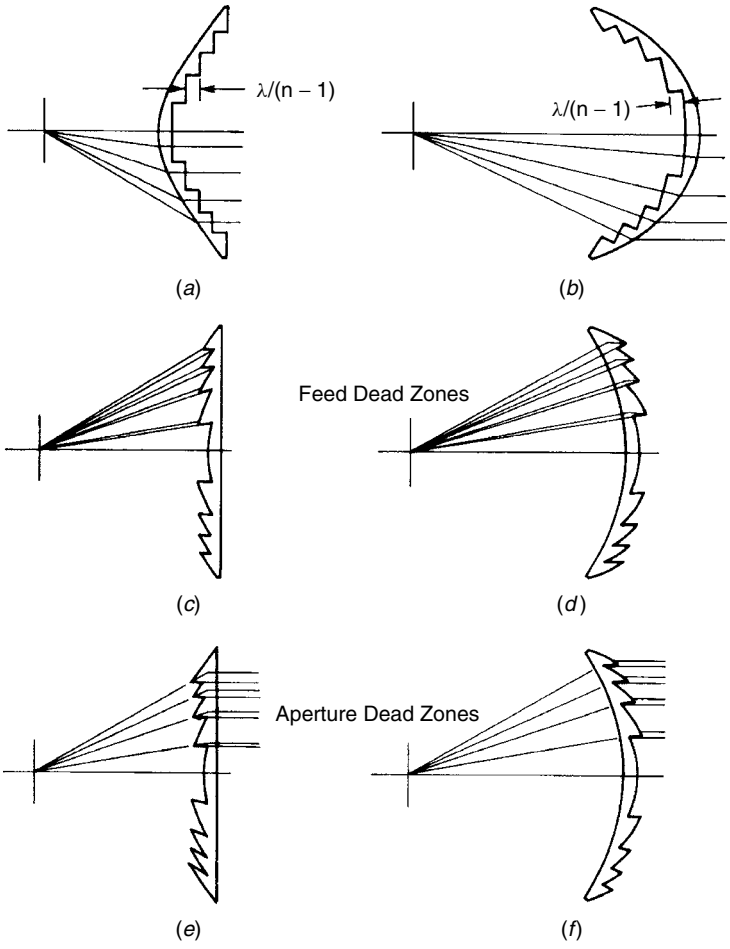

FIGURE 9-2 Zoning of single-surface lenses.

for each inner step of hyperbolical lenses and decreases by the same amount for each inner step of elliptical lenses. We derive the lens-induced taper relative to the center by using ratios of Eq. (9-13) or (9-14). For axisymmetrical lenses,

$$\frac{A(r,\phi)}{A_c} = \begin{cases} \dfrac{f_c^2(n\cos\psi - 1)^3}{f^2(n-1)^2(n-\cos\psi)} & \text{hyperbolical} \quad (9\text{-}18) \\ \dfrac{f_c^2(n-\cos\psi)^3}{f^2(n-1)^2(n\cos\psi - 1)} & \text{elliptical} \quad (9\text{-}19) \end{cases}$$

where f_c is the focal length in the center, f the focal length in the feed direction ψ, and A_c the central amplitude.

Example Design an axisymmetrical hyperbolical lens ($n = 1.6$) by using the three types of zoning shown in Figure 9-2, using an aperture diameter of 30λ and a maximum feed angle of 35° with a 70° 10-dB beamwidth feed.

The minimum allowable thickness is 0.5λ with a 0.3λ edge thickness. By working through the geometry, we obtain dimensions for the following cases:

Figure 9-2a, nonrefracting surface zoning, we compute steps $= \lambda/(n-1) = 1.67\lambda$.

Step	1	2	3	4
Aperture Radius (λ)	12.418	10.009	7.403	4.256

We estimate the feed spillover loss from Eq. (8-12) for the 10-dB feed edge taper, 0.41 dB. Equation (9-15) gives the edge taper (9.72 dB), since the refracting surface is not zoned. Combined with the feed edge taper of 10 dB, we have a 19.72-dB amplitude taper in the aperture plane. We use Eq. (4-8) to calculate the amplitude taper loss (1.8 dB) for this axisymmetric distribution.

Figure 9-2c, zoning in the refracting surface of the hyperbolical lens (parallel with outgoing waves), we compute the dimensions starting with the edge focal length found from a rearrangement of Eq. (9-4) (Table 9-1). The changing focal lengths in the zones alter the aperture amplitude distribution. The edge taper becomes [Eq. (9-18)] 6.24 dB and reduces the amplitude taper loss [Eq. (4-8)] to 1.19 dB. The portion of the feed directed to the dead zones refracts out of the aperture and forms sidelobes that reduce the aperture efficiency. We consider this as a second spillover loss (0.81 dB).

Figure 9-2e, zoning in the refracting surface of the hyperbolical lens (parallel with the feed wave rays), again we start with the edge focal length and increase it by $\lambda/(n-1)$ at each step and determine the feed angles where the change in the focal length will give the minimum allowable thickness. The dimensions given in Table 9-2 were obtained. Since the focal lengths are the same as for Fig. 9-2*c*, the lens-induced edge taper is 6.24 dB. The dead zones in the aperture distribution increase the amplitude taper loss to 3.10 dB. These ring dead zones can be considered as radiating and adding to the fully excited aperture pattern. They radiate patterns with closely spaced lobes that raise the near sidelobes of the total antenna. The three designs are compared in Table 9-3.

Example Similar to the example above, we can design zoned elliptical axisymmetrical lenses that have the same problems of feed angle or aperture dead zones.

The edge taper of the elliptical lens counteracts some of the feed taper and reduces amplitude taper loss. The losses calculated for those designs are given in Table 9-4.

TABLE 9-1 Zoned Hyperbolical Lens, Figure 9-2*c*

Zone	Focal Length (λ)	Aperture Radius of Step (λ)	Thickness (λ)	Feed Dead Zone Angles (deg)
1	20.21	0	1.52	
2	18.54	5.12	2.09	13.57–14.02
3	16.87	8.42	1.98	21.64–23.10
4	15.21	10.84	1.90	27.06–28.68
5	13.54	12.89	1.83	31.28–32.95

TABLE 9-2 Zoned Hyperbolical Lens, Figure 9-2*e*

Zone	Focal Length (λ)	Feed Angle (deg)	Thickness (λ)	Aperture Dead Zones (λ)
1	20.21	0	1.51	0
2	18.54	13.57	2.25	4.70–5.12
3	16.87	21.64	2.41	7.66–8.42
4	15.21	27.06	2.60	9.77–10.84
5	13.54	31.28	2.83	11.48–12.89

TABLE 9-3 Aperture Illumination Losses of Three Hyperbolical Lenses, Figure 9-2

Design (Figure 9-2)	*SPL* (dB)	*ATL* (dB)	Sum (dB)
(*a*)	0.41	1.80	2.21
(*c*)	1.22	1.19	2.41
(*e*)	0.41	3.10	3.51

TABLE 9-4 Aperture Illumination Losses of Three Elliptical Lenses, Figure 9-2

Design (Figure 9-2)	*SPL* (dB)	*ATL* (dB)	Sum (dB)
(*b*)	0.41	0.06	0.47
(*d*)	1.43	0.14	1.57
(*f*)	0.41	1.43	1.84

Zoning reduces the frequency bandwidth. At the center frequency the optical path length difference between the central ray and edge ray is $K - 1$ for K zones. A common maximum allowed deviation of feed to aperture path is 0.125λ, which leads to a bandwidth of

$$B \simeq \frac{25\%}{K - 1} \tag{9-20}$$

For the five zone lenses of the examples above, Eq. (9-20) gives a 6% bandwidth. We determine the loss at band edge by tracing rays from the feeds-to-aperture plane and calculating the phase error loss using Eq. (4-9). The loss at band edge is about 0.3 dB for all the designs. Bandwidth is greatly underestimated by Eq. (9-20) if a greater phase error loss is allowed. The 1-dB phase error loss bandwidth is $45\%/(K - 1)$.

9-3 GENERAL TWO-SURFACE LENSES

Optical lens designs use either flat or spherical surfaces, an approximation useful for long focal lengths. We design lenses exactly. In Section 9-1 we discussed lenses where the rays refracted at only one surface. The shape curve of these two lenses could be

derived easily. In this section we pick the curve for one lens surface and use a numerical search for the second surface that generates a table of (r, z) values. We generate a cubic spline from the table and use it to calculate the surface normal vector and the radius of curvature useful in manufacture. The initial numerical search generates ray paths through the lens that produce a table of feed angle versus aperture radius. We apply Eq. (9-11) to compute the aperture distribution after we generate the cubic spline whose evaluation includes the derivative.

If we specify the surface on the feed side, we start at the feed and trace rays to the inner surface. We know the inner surface normal vector because it is a specified surface. We compute the direction of the ray inside the lens given the incident medium index of refraction n_i, n_o inside the lens, the surface unit normal $\mathbf{n}$ directed into the lens, and the incident ray unit vector $\mathbf{S}_i$. First determine if the ray will exit the incident ray medium, because if $n_i > n_o$, it can act as a prism and have total reflection:

$$R_a = n_o^2 - n_i^2[1 - (\mathbf{S}_i \cdot \mathbf{n})^2]$$

If $R_a < 1$, the ray is totally reflected. For $R_a > 1$, we determine the direction of the output ray unit vector $\mathbf{S}_o$ from the following operations [3, p. 355]:

$$\gamma = \sqrt{R_a} - n_i \ (\mathbf{n} \cdot \mathbf{S}_i) \qquad \text{find the vector } \mathbf{t} = n_i \mathbf{S}_i + \gamma \mathbf{n} \qquad \mathbf{S}_o = \frac{\mathbf{t}}{|\mathbf{t}|} \tag{9-21}$$

For our case the normal vector, incident, and refracted rays are in two-dimensional space (z, r), because the lens has axisymmetry. To start, specify the z-axis distance from the feed to the outer rim of the lens, the initial radius, and the rim thickness along the initial internal ray direction. The feed-side position of the lens is (z_1, r_1). Apply Eq. (9-21) and find the outer lens point given the rim thickness t_r, by tracing along the vector $\mathbf{t}$ to point (z_2, r_2). Since the lens collimates the beam, we trace the ray to a plane $z = z_3$ whose normal is the z-axis. Figure 9-3 illustrates the rim and internal ray paths for a lens with a spherical inner surface. We calculate the electrical path length from the feed located at $z = z_f$ to the output plane by including the index

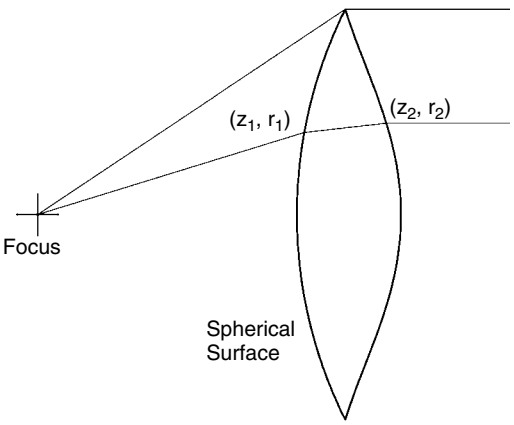

FIGURE 9-3 Ray tracing in a single-surface lens with a specified spherical inner surface.

of refraction n of the lens for the ray path length (PL) through the lens, and the input and output ray lengths:

$$\text{PL} = \sqrt{r_1^2 + (z_1 - z_f)^2} + n\sqrt{(r_2 - r_1)^2 + (z_2 - z_1)^2} + (z_3 - z_2) \tag{9-22}$$

The design consists of stepping in r_1, tracing the ray to the inner lens surface, computing the direction of the ray internal by Eq. (9-21), and determining thickness t_r when Eq. (9-22) minus the initial path length is zero. By Fermat's principle of equal path length, the outer surface refraction direction adds to the inner surface refraction to produce parallel output rays. This procedure generates a table of (z_2, r_2) pairs that we convert to a cubic spline. By using the cubic spline, we produce an evenly spaced table of (z_2, r_2) for machining, and if necessary, a table of radius of curvature from the second derivative to assist machining operations. The next step is to calculate a cubic spline between the aperture radius r_2 and the feed angle ψ because its output includes $d\psi/dr_2$. By rearranging Eq. (9-11), we compute the aperture power distribution given the feed power pattern:

$$A(r_2, \phi) = \frac{F(\psi, \phi) \sin \psi}{r_2} \frac{d\psi}{dr_2} \tag{9-23}$$

The design steps for a lens with the outer surface specified are similar except that we trace rays from the output plane backward to the feed point. Again, we start at the lens rim, use Eq. (9-21) to calculate the internal ray direction by using the $-z$-directed ray and the known surface normal to travel along this ray by the rim thickness to the inner surface. Equation (9-22) gives the electrical path length for this lens, as well. We repeat the root-finding procedure used above to determine a series of points (z_1, r_1) along the surface by equating all electrical path lengths. We generate the same series of cubic splines to obtain machining dimensions and differential $d\psi/dr_2$ used in Eq. (9-23) for the aperture power distribution. Figure 9-4 shows the aperture distributions for various lenses with focus points located 1.5 times the radius below the lens. The curves include lenses of Section 9-1.

The focal spot is not a singularity as drawn on the figures using geometric optics, but spreads due to the finite wavelength. We use Gaussian beams to evaluate the size of focal spots. For a lens with a collimated output, we assume a Gaussian beam on the output with minimum waist diameter $2W_0 = D$, the lens diameter, radiating into free space, and a matching Gaussian beam on the feed side which tapers to the focal plane. The lens transforms one Gaussian beam into another. The focal length $f = z_f$ and we determine the diameter of the focal spot $2W_0'$ and the half depth of focus b from the lens F-number $F_\# = f/D$ [4, pp. 91–95]:

$$2W_0' = \frac{4\lambda}{\pi} F_\# = \frac{4\lambda}{\pi} \frac{f}{D} \qquad b = \frac{8\lambda}{\pi} F_\#^2 \tag{9-24}$$

A small modification to Eq. (9-22) allows the design of lenses with a second focus at a finite position $z = z_3$ on the axis:

$$\text{PL} = \sqrt{r_1^2 + (z_1 - z_f)^2} + n\sqrt{(r_2 - r_1)^2 + (z_2 - z_1)^2} + \sqrt{r_2^2 + (z_3 - z_2)^2} \tag{9-25}$$

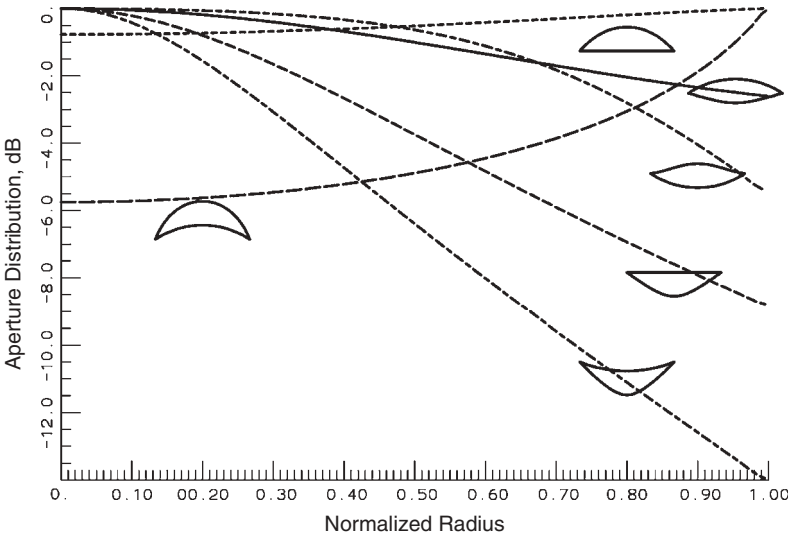

FIGURE 9-4 Aperture distribution for various single-surface lenses with $f/D = 1.5$.

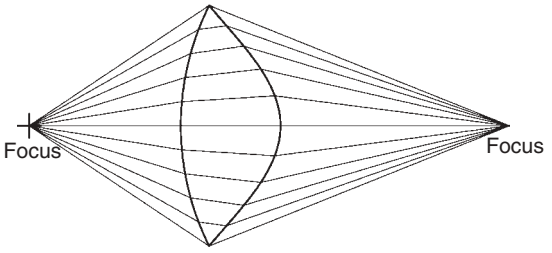

FIGURE 9-5 Ray tracing in lens designed for two finite focuses.

We follow the same steps as in the design above except that we need to generate a table of feed angles given the output ray angle with respect to the z-axis. Figure 9-5 illustrates a typical design and shows the ray tracing.

The lens designs noted above narrow the beamwidth. We design lenses to spread the beam by using a virtual focus located behind the output surface of the lens, as shown in Figure 9-6. Because the rays trace backward to the virtual focus, we change the sign of the last term in Eq. (9-25):

$$\text{PL} = \sqrt{r_1^2 + (z_1 - z_f)^2} + n\sqrt{(r_2 - r_1)^2 + (z_2 - z_1)^2} - \sqrt{r_2^2 + (z_3 - z_2)^2} \qquad (9\text{-}26)$$

The iterative design procedure should be modified to start in the center of the lens because the concave lens has a significant outer thickness. We compute focal length f of the lens by the distance of the two focuses from the lens:

$$\frac{1}{f} = \frac{1}{z_f} + \frac{1}{z_3} \qquad (9\text{-}27)$$

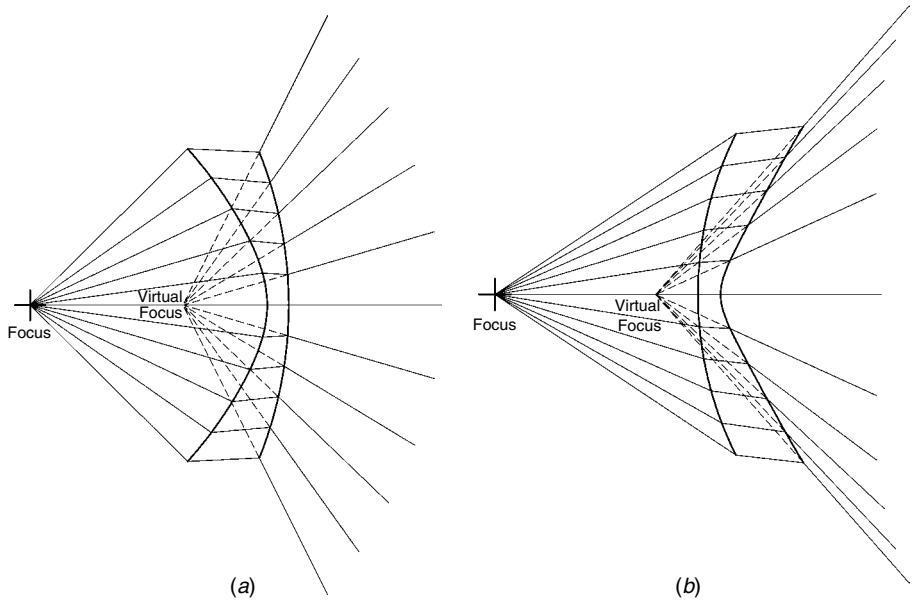

FIGURE 9-6 Lenses designed with virtual focuses to widen beam: (*a*) spherical outer surfaces; (*b*) spherical inner surfaces.

To calculate the pattern we trace rays through the lens either to a planar surface output side of the lens or the actual surface. By using a cubic spline between the feed angle and the aperture position we calculate the amplitude due to spreading [Eq. (9-23)]. We replace the fields with currents and use physical optics to calculate the pattern. A second simpler approach uses a Gaussian beam approximation for lenses that accounts for electrical size. Both the input and output Gaussian beam have the same waist at the lens plane. Each Gaussian beam decreases in a hyperbola to the minimum waist at the location of the phase center or focus. The output does not pass through a narrow caustic, as shown in Figure 9-5, but reaches a finite-diameter waist related to the feed beamwidth and the lens diameter.

At this point we design the lenses scaled to wavelengths. Given the feed beamwidth, we calculate the half depth of focus b by using Eq. (7-35). The lens magnifies the output beam waist compared to the input beam waist by M. First, we calculate an input magnification factor M_r:

$$M_r = \left| \frac{f}{z_f - f} \right| \tag{9-28}$$

With b given in wavelengths, we compute the ratio of b to the shift of the feed relative to the focus:

$$r = \frac{b}{z_f - f} \tag{9-29}$$

We combine Eqs. (9-28) and (9-29) to calculate the lens magnification M:

$$M = \frac{M_r}{\sqrt{1 + r^2}} \tag{9-30}$$

The output Gaussian beam propagates from the second focus with new parameters: b', the half depth of focus, waist W_0', and divergence angle θ_0' [4]:

$$b' = M^2 b \qquad W_0' = M W_0 \quad \theta_0' = \frac{\theta_0}{M} \tag{9-31}$$

Example The lens in Figure 9-5 was designed for a diameter of 20λ, $z_f = 15\lambda$, and $z_3 = 25\lambda$. We calculate the focal length from Eq. (9-27) as $f = 9.375\lambda$. A feed with a 68° 10-dB beamwidth is approximated by a Gaussian beam with $b = 0.99\lambda$ (Scale 7-8) and $2W_0 = 1.12\lambda$ (Scale 7-9). We use b to find the magnification M by using Eqs. (9-28) to (9-30), $M = 1.64$. The Gaussian beam at the second focus has a minimum waist $2W_0' = 1.64(1.12) = 1.84\lambda$. Using Scales 7-7 to 7-9, we read the Gaussian beam output values: 10-dB beamwidth = 42°(gain = 18.4 dB). Scale 7-7 gives the gain of the feed as 14.3 dB. The half depth of focus increased from 0.99λ to 3.39λ.

Example When we repeat the lens calculations for the lens of Figure 9-6*a* for a diameter = 20λ, $z_f = 15\lambda$, and $z_3 = -5\lambda$, we calculate $f = -7.5$. Starting with a feed 10-dB beamwidth = 80°, we use Scale 7-8 to find $b = 0.7\lambda$ and waist diameter $2W_0 = 0.94\lambda$. The negative focal length produces a magnification below 1: $M = 0.333$. This decreases b to 0.0775λ and $2W_0' = 0.314$. The output Gaussian beam gain drops to 6.6 dB from a feed gain of 12.9 dB.

9-4 SINGLE-SURFACE OR CONTACT LENSES

We can alter the pattern of antennas with planar surfaces such as spirals and microstrip patches by placing a lens directly on the planar surface. The lens can be spaced a small distance away to avoid potential damage and have little pattern impact. The lens modifies the original pattern of the antenna by using the refraction at the single output surface. Because the lens contacts the antenna, the pattern inside the lens is the same as radiated into free space except for the dielectric loading on the antenna. This loading shifts the operating frequency and in the case of a spiral improves its efficiency and widens its beamwidth (see Section 11-5.1).

We design these antennas by first generating a mapping between the feed angle ψ and the output angle θ. This could be as simple as $\theta(\psi) =$ constant or a function to generate a shaped beam, in the same manner as a shaped reflector (see Section 8-20). The relationship $\theta\ (\psi)$ enables calculation of the surface normal at every point along the outer surface. The surface normal is found from the gradient of the radial vector, and equating the two values produces a differential equation between the radius r and the feed angle ψ. Given the feed angle and the output angle at a point on the lens, we calculate the surface normal from $\mathbf{n} = n\mathbf{S}_i - \mathbf{S}_o$, where n is the index of refraction, $\mathbf{S}_i$ the incident unit vector, and $\mathbf{S}_o$ the exiting ray unit vector. We normalize $\mathbf{n}$ to a vector $\mathbf{v}$. The gradient of $r(\psi)$ gives a second expression for the normal vector:

$$\nabla r(\psi) = \mathbf{a}_r + \mathbf{a}_\psi \frac{1}{r(\psi)} \frac{\partial r(\psi)}{\partial \psi} \tag{9-32}$$

The coefficient of $\mathbf{a}_\psi$ in Eq. (9-32) is the tangent of the angle α between the normal vector and the radial vector (incident ray). The tangent can be found from the unit

vector $\mathbf{v}$ and the incident ray unit vector $\mathbf{S}_i$:

$$\tan\alpha = \frac{(\mathbf{S}_i \times \mathbf{v})}{\mathbf{S}_i \cdot \mathbf{v}} = \frac{1}{r(\psi)} \frac{\partial r(\psi)}{\partial \psi} \tag{9-33}$$

The cross product between the incident ray and the unit vector $\mathbf{v}$ only has a z-axis component, because the incident ray and the surface normal lie in the $x-y$ plane. We design the lens surface by solving the differential equation (9-33). A numerical technique such as the Runge–Kutta method easily solves the equation when we start at one feed angle and an arbitrary lens radius and step through feed angles. The method determines only the shape of the lens to an arbitrary size that we scale to the diameter desired.

Figure 11-9*a* illustrates a lens designed to redirect all feed rays to $\theta = 0$. Figure 9-7 illustrates the shape of a contact designed to redirect all rays between feed angles 0 through 60° to output rays at 30°. For a 3λ lens diameter and a feed 12-dB beamwidth of 120°, the lens spreads the beam to form a flat-topped output beam shown in Figure 9-8. Contact lenses can greatly modify radiation from a feed with electrically small lenses.

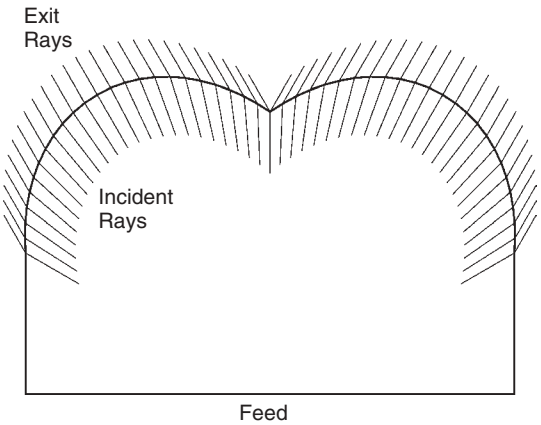

FIGURE 9-7 Contact lens designed to direct the beam in a cone at 30°.

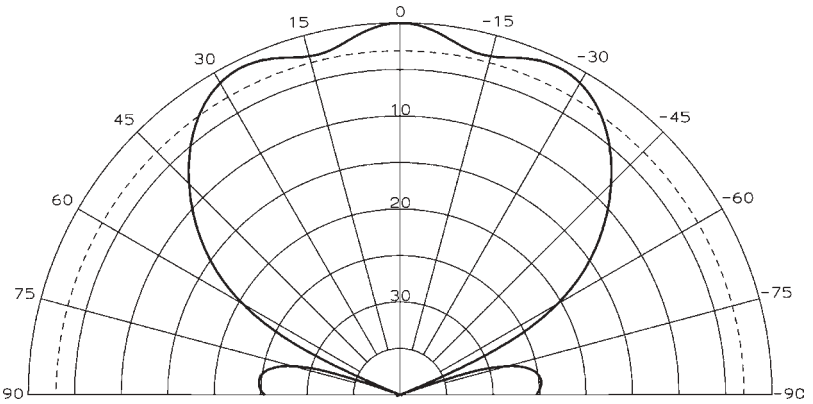

FIGURE 9-8 Pattern of contact 3λ-diameter lens for a feed with a 12-dB beamwidth of 120°.

9-5 METAL PLATE LENSES

The phase velocity of a wave in waveguide exceeds that of a wave in free space and produces a medium with an effective refractive index of less than 1. We can make a microwave lens by spacing parallel metal plates and feeding the lens with a wave polarized in the direction of the plates. For plates spaced a distance a, the index of refraction is

$$n = \sqrt{1 - \left(\frac{\lambda}{2a}\right)^2} \tag{9-34}$$

where λ is the wavelength in the medium between the plates. The index of refraction is frequency dependent. The lens can be made polarization independent by forming an egg crate of orthogonal plates. We divide an arbitrary polarization into orthogonal polarizations normal to each set of plates.

If we substitute n from Eq. (9-34) into Eq. (9-1), we obtain the equation of a front single-surface lens:

$$\rho(\psi) = \frac{(1-n)f}{1 - n\cos\psi} \tag{9-35}$$

Equation (9-35) is an ellipse with f as the distance from the far focus of the ellipse to the center of the lens front surface. This surface refracts waves parallel with the axis and determines the second surface: a plane. The parallel plates constrain the waves parallel with the axis and prevent the design of an outer single-surface lens.

The cutoff wavelength $2a$ and the possibility of higher-order modes restrain the range of n. The second-order-mode cutoff occurs when $\lambda = a$, and it limits n to 0.866 [Eq. (9-34)]. At cutoff, $\lambda = 2a$ and n equals zero. Reasonable values lie between 0.3 and 0.7.

The variation of n versus frequency limits bandwidth. When the phase variation in the aperture is limited to $\lambda/8$, the bandwidth is approximately [1]:

$$\text{bandwidth}(\%) = \frac{25n}{1-n}\frac{\lambda}{(1-n)t} \tag{9-36}$$

where n is the center-frequency index of refraction and t is the maximum thickness. An acceptable bandwidth is underestimated by Eq. (9-36) through restriction of the band edge phase error.

The elliptical surface increases the aperture distribution toward the edges. When we substitute Eq. (9-35) into Eqs. (9-11) and (9-12), we obtain the aperture amplitude distribution relative to the feed pattern:

$$\frac{A(r,\phi)}{F(\psi,\phi)} = \frac{(1-n\cos\psi)^3}{f^2(1-n)^2(\cos\psi - n)} \qquad \text{axisymmetrical}$$

$$\frac{A(r,y)}{F(\psi,y)} = \frac{(1-n\cos\psi)^2}{f(1-n)(\cos\psi - n)} \qquad \text{cylindrical} \tag{9-37a, b}$$

Example Design an axisymmetric parallel-plate lens with a diameter of 30λ, maximum feed angle of 35°, $n = 0.625$, and minimum thickness of λ.

$$\rho(35^\circ) = \frac{30\lambda}{2\sin 35^\circ} = 26.15\lambda$$

Rearrange Eq. (9-35) to calculate the focal length at the edge:

$$f = \frac{(1 - n\cos 35^\circ)\rho(35^\circ)}{1 - n} = 34.03\lambda$$

Equation (9-34) gives us the plate separation with a slight rearrangement:

$$a = \frac{1}{2\sqrt{1 - n^2}} = 0.64\lambda$$

The amplitude variation from the center to the edge caused by the ellipse is given by Eq. (9-37*a*):

$$\frac{A(\psi_e)}{A(0)} = \frac{(1 - n\cos\psi_e)^3}{(1 - n)^2(\cos\psi_e - n)} = 4.26 \quad (6.3\,\text{dB})$$

A feed with its 10-dB beamwidth equal to the subtended angle of the lens at the feed produces −3.7 dB edge taper in the aperture. The edge thickness is given by

$$t = f + 1 - \rho(35^\circ)\cos(35^\circ) = 13.61\lambda$$

Equation (9-36) predicts a bandwidth of 1.9%. A detailed analysis using ray tracing through the lens and varying n with changes in frequency predicts a 0.2-dB loss at this band edge. The 1-dB bandwidth is about 4.5%.

Zoning a parallel-plate lens increases its bandwidth by limiting the maximum thickness, since the variation of the optical path length due to the varying n exceeds that due to the zoning. Figure 9-9 gives the central curve of the three possible types of zoning. The lens in Figure 9-9*a* only suffers loss due to diffractions from edges. The other two zoned lenses (Figure 9-9*b, c*) have dead zones in the aperture. These dead zones produce additional amplitude taper loss and high close-in sidelobes.

The feed-side zoning has different focal lengths in each zone. The outer zone remains the same as the unzoned lens. The focal lengths of the inner zones are reduced by $\lambda/(1 - n)$ at each step and the stepping reduces the amplitude taper of the lens by varying f:

$$\frac{A(\psi)}{A(0)} = \frac{f_c^2(1 - n\cos\psi)^3}{f^2(1 - n)^2(\cos\psi - n)} \tag{9-38}$$

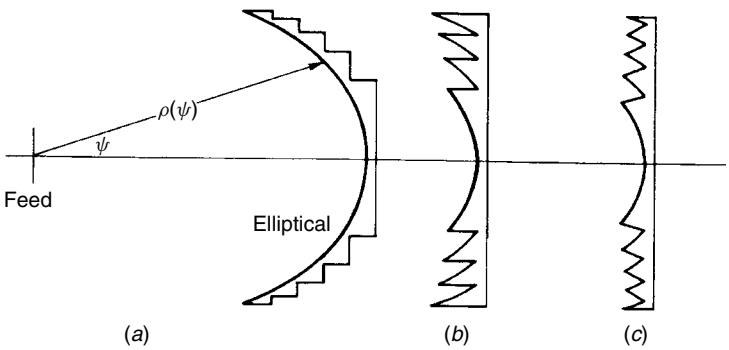

FIGURE 9-9 Central section of zoned parallel metal plate lenses.

where f_c is the central focal length and f is the focal length of the ellipse at ψ. The zoned lens bandwidth is approximately [1]

$$\text{BW} = \frac{25\%}{K - 1 + [(1+n)(1-n)t/n]} \tag{9-39}$$

where K is the number of zones and t is the maximum thickness. Equation (9-39) also is an underestimation of an acceptable loss-level bandwidth.

Example The lens of the example above was zoned as in Figure 9-9*a* and *c* with five zones. The maximum thickness is 3.4λ. Equation (9-39) predicts a bandwidth of 3.4%. By tracing rays through the lens and applying Eq. (4-9) to calculate phase error loss, we predict a 10% bandwidth for a 1-dB loss.

Zoning the nonrefracting surface has no effect on the aperture distribution except for edge diffractions that modify the fields slightly. Zoning the refracting surfaces causes aperture dead zones and reduces the lens-induced amplitude taper. The focal length of the ellipse at the edge remains at 34.03λ. The focal length of the center ellipse is reduced by $4\lambda/(1-n)$ from the edge ellipse to 23.36λ. The edge taper [Eq. (9.38)] becomes 2.01 (3 dB). The aperture dead zones increase the loss by 2 dB.

The bandwidth of a parallel-plate lens can be increased by a method of compounding lenses into a doublet [5]. We can make a lens by using a uniform waveguide length between the input and output surfaces and placing a phase shifter in each line to compensate for the optical path-length differences and produce an eikonal at the aperture plane. If we combine a refracting surface waveguide plate lens with a differential phase shift lens, we can match the aperture phase at two frequencies. This matching broadbands the antenna like an optical achromatic doublet.

9-6 SURFACE MISMATCH AND DIELECTRIC LOSSES

The reflection coefficient of a wave normally incident on a dielectric is

$$\Gamma = \frac{1-n}{1+n} \tag{9-40}$$

valid for both dielectric and metal lenses. The actual reflection coefficient of any ray depends on the angle of incidence and the polarization. Both surfaces of the lens have reflections, and these interact to produce the actual reflection. With plane surfaces, such as those assumed for radomes, we can analyze the combination of reflections using transmission-line mismatch equivalence. Since the reflections from second surfaces may not return to the same point as the incident waves and may have their caustic distances changed by the curved surfaces, transmission-line models of the two surfaces have limited use for lenses. Equation (9-40) gives us a reasonable approximation to expected mismatch, since one surface of the single refracting surface lens will be normal to the wave incident from the feed and reflect into the feed. The second surface fails to focus power back to the feed and has a minor effect.

Example A lens with $n = 1.6$ or $n = 0.625$ has a reflection coefficient magnitude of 0.23 [Eq. (9-40)] at one surface that focuses into the feed. This gives a feed mismatch if

$$\text{VSWR} = \frac{1 + 0.23}{1 - 0.23} = 1.6$$

the same as n ($n > 1$) or $1/n$ ($n < 1$). The mismatch loss becomes $1 - |\Gamma|^2 = 0.95$ (0.2 dB).

The wave may be matched to the surface by a quarter-wavelength transformer with an index of refraction $n^{1/2}$, but adding matching transformers narrows the bandwidth. The surface, which reflects power back to the feed, should be matched first, since the second surface has a minor effect on feed mismatch. Also, the primary reflecting surface has normally incident waves and does not suffer from the need to vary the thickness to match waves off normal incidence. Transformers to match waves off normal incidence are polarization-sensitive.

Simple methods can be used to reduce lens-caused feed mismatch [2]. The lens can be tilted to cause the reflection to miss the feed. Offsetting half the lens by $\lambda/4$ causes cancellation of the reflection from the two halves. Tilting does not reduce the mismatch loss but does produce backlobe power in the pattern. Similarly, the reflected power from the hyperbolical surface forms backlobes. These reflections reduce the antenna efficiency below that predicted by aperture theory alone.

Cohn and Morita [2,6] developed methods of matching the surface of the lenses by removing some of the dielectric for a quarter wavelength. The surfaces are either corrugated, have arrays of holes, or have arrays of rods. With this method, the lens can be made from a single dielectric slab. The design depends on the angle of incidence and the polarization of the waves. The lens dissipates power by the attenuation constant of the material:

$$\alpha = \frac{27.3n \tan \delta}{\lambda} \qquad \text{dB/length} \tag{9-41}$$

where $\tan \delta$ is the loss tangent of the dielectric. Waveguide losses reduce the power transmitted through metal plate lenses. Zoning eliminates material and its associated loss to improve efficiency, but for most materials, this effect is small.

Artificial dielectrics [2] reduce excessive weight and material losses of lenses. We make them by embedding metal particles or plated microspheres in foam with a dielectric constant near 1. The metal parts may be strips or disks made from metal foil. Similarly, solid metal parts can be hollow. Since the effective dielectric constant depends on the size of the metal particles in wavelengths, lenses made from artificial dielectrics will be narrowband if the particles are large, but the use of plated microspheres dispersed in the foam reduces this problem.

9-7 FEED SCANNING OF A HYPERBOLOIDAL LENS [7]

The hyperboloidal lens has no cross-polarization when fed from an electric dipole source. Kreutel [7] analyzed the effects of off-axis dipole sources on the pattern of the hyperboloidal lens. The coma increases more rapidly for the lens than for a paraboloidal reflector for the same scanning. Like the paraboloidal reflector, the hyperboloidal lens beam scans less than the deviation angle of the feed relative to the vertex and axis and has a beam deviation factor (Table 9-5). The scanning loss (Table 9-6) decreases with increasing n. The peak coma lobe (Table 9-7) limits the possible scan before unusable patterns are obtained. The paraboloidal reflector can be scanned further (Table 8-2) for the same coma.

TABLE 9-5 Beam Deviation Factor for a Feed-Scanned Hyperboloidal Lens

f/D	$n=\sqrt{2}$	$n=2$	f/D	$n=\sqrt{2}$	$n=2$	f/D	$n=\sqrt{2}$	$n=2$
0.8	0.75	0.84	1.4	0.86	0.91	2.0	0.93	0.95
1.0	0.80	0.87	1.6	0.89	0.92	2.5	0.95	0.96
1.2	0.83	0.89	1.8	0.92	0.94	3.0	0.97	0.98

TABLE 9-6 Scanning Loss for a Hyperboloidal Lens (dB)

Beamwidth of Scan	$n=\sqrt{2}$		$n=2$	
	$f/D=1$	$f/D=2$	$f/D=1$	$f/D=2$
0.5	0.03	0.00	0.01	0.00
1.0	0.06	0.01	0.04	0.01
1.5	0.12	0.03	0.07	0.02
2.0	0.23	0.05	0.12	0.04
2.5	0.36	0.09	0.20	0.06
3.0	0.51	0.13	0.28	0.08
3.5	0.69	0.19	0.37	0.11
4.0	0.90	0.24	0.49	0.14
4.5	1.09	0.31	0.60	0.18
5.0		0.38	0.75	0.22
5.5		0.44		0.25

TABLE 9-7 Coma Sidelobe Level for a Scanned Hyperboloidal Lens (dB)

Beamwidth of Scan	$n=\sqrt{2}$		$n=2$
	$f/D=1$	$f/D=2$	$f/D=1$
0	20.9	18.5	19.5
1	17.6	17.5	17.6
2	15.2	16.5	15.7
3	13.1	15.5	14.2
4	11.3	14.8	12.9
5	9.8	14.0	11.5
6	8.8	13.3	10.4

9-8 DUAL-SURFACE LENSES

The second surface of the lens offers an additional degree of freedom that can be used to control the pattern characteristics. Ruze [8] developed methods to reduce coma for feed-scanned cylindrically shaped metal plate lenses, which constrain the wave parallel with the axis. Both surfaces are used to satisfy focusing requirements. We will develop a method for axisymmetrical dielectric lenses to eliminate coma for small feed

displacements. In a second design we can also use the second surface shape to control the amplitude distribution in the aperture plane.

9-8.1 Coma-Free Axisymmetric Dielectric Lens [9]

The design of the coma-free axisymmetric antenna reduces to the numerical solution of a differential equation with side conditions to produce a collimated beam and satisfy the Abbe sine condition [10, p. 157]. Successful designs require a number of iterations, since the ultimate lens shape depends heavily on the initial conditions. Solution of the differential equation will sometimes diverge into unrealizable designs or fail to continue to satisfy the side conditions.

A lens satisfying the Abbe sine condition is free of coma aberrations for small deviations of the feed from the axis. The deviations produce higher-order aberrations that eventually distort the beam with continued scanning, but coma is removed. For a lens focused at infinity, the Abbe sine condition requires that the surface which refracts the waves parallel with the axis must be spherical with its center on the effective focus of the lens. The dielectric lens refracts waves parallel with the axis on the outer surface (away from the feed). Given the aperture radial component r,

$$r = f_e \sin \psi \tag{9-42}$$

where f_e is the effective focus and ψ is the feed angle. A waveguide plate lens satisfies the Abbe sine condition by having a spherical inner surface [6], since the waves are parallel with the axis in the lens because the waveguide plates constrain the wave to be parallel with the axis.

The second surface must produce the conditions for a uniform phase in the aperture plane. The waveguide plate lens only has to equalize path lengths. In a dielectric lens, the inner surface must refract the waves in the proper direction to satisfy the Abbe sine condition, and it must be so placed as to equalize the path lengths from the feed to the aperture plane. The locations of both surfaces along the axis are varied to equalize the path lengths.

Figure 9-10 shows the coordinates of the coma-free dielectric lens. The polar equation $\rho\ (\psi)$ describes the inner surface and ψ' is the angle of the refracted wave with the axis. The distance from the feed to the center of the lens inner surface is f, and T is the thickness. The coordinates (r, z) describe the outer lens surface, where z is the axis dimension and r is the aperture radial component. Snell's law reduces to a differential equation at the inner surface:

$$\frac{d\rho}{d\psi} = \frac{n \sin(\psi - \psi')\rho}{n \cos(\psi - \psi') - 1} \tag{9-43}$$

where

$$\tan \psi' = \frac{r - \rho \sin \psi}{z - \rho \cos \psi} \tag{9-44}$$

By use of Eq. (9-42), this reduces to

$$\tan \psi' = \frac{(f_e - \rho) \sin \psi}{z - \rho \cos \psi} \tag{9-45}$$

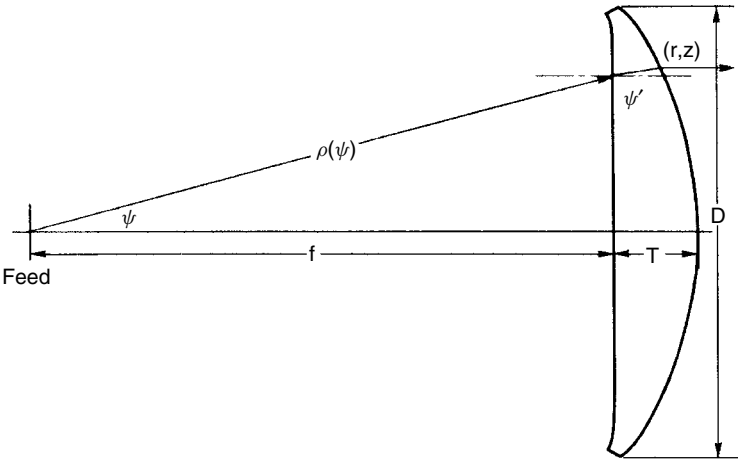

FIGURE 9-10 Coma-corrected dual-surface axisymmetric lens; $n = 1.6$, $D = 35$, $f = 45$, $T = 6.5$, $f_e = 49$.

The requirement for equal optical path lengths to the aperture determines a quadratic equation in z:

$$Az^2 + Bz + C = 0 \tag{9-46}$$

where

$$A = n^2 - 1$$
$$B = 2(\rho - K) - 2n^2\rho\cos\psi$$
$$C = n^2\rho^2\cos^2\psi + n^2(f_e - \rho)^2\sin^2\psi - (\rho - K)^2$$
$$K = T(n-1)$$
$$z = \frac{-B + \sqrt{B^2 - 4AC}}{2A}$$

Design consists of the numerical solution of the differential equation (9-43) subject to the conditions of Eqs. (9-45) and (9-46). Realizable solutions depend on the initial conditions. Most failures to produce a usable design occur in Eq. (9-46), which satisfies the requirement of equal aperture phase.

Example Figure 9-10 shows a scale drawing of a realizable design for $n = 1.6$, focal distance $f = 45$, diameter $D = 35$, center thickness $T = 6.5$, and effective focal length $f_e = 49$. Table 9-8 lists a few points of the solution obtained by a Runge–Kutta numerical method for the differential equation (9-43).

The example above contains only relative dimensions. The solution is size and frequency independent, since it is obtained by geometric optics. We can zone the lens for a given frequency by cutting along ray paths. Each step is $\lambda/(n-1)$. Table 9-8, as in the example above, determines the ray paths through the lens. Zoning will produce either feed or aperture dead zones. The reduction of weight must be balanced with

TABLE 9-8 Design of Figure 9-11 for a Coma-Free Lens

Feed Angle, ψ (deg)	Inner Surface, $\rho(\psi)$	Horizontal Distance, z	Radius, r	Thickness Along Ray, T
0	45.00	51.50	0	6.50
5	45.18	51.19	4.27	6.20
10	45.70	50.27	8.51	5.29
15	46.59	48.71	12.68	3.77
20	47.63	46.28	16.76	1.59
20.92	47.61	45.40	17.50	1.06

the loss in efficiency to achieve some compromise. Because we used the degrees of freedom of the second surface to satisfy the Abbe sine condition, we lose control of the aperture distribution through the lens surfaces. Most practical designs produce an amplitude taper near that of the feed antenna. We must achieve low sidelobes, if required, through a tapered illumination from the feed. The feed pattern plays no part in the design and gives us degrees of freedom for amplitude taper. An antenna designed and built with a diameter of 32 wavelengths [9] showed no coma in a scanning of ± 2 beamwidths. Like the paraboloidal reflectors, increasing the focal length for a given diameter allows greater scanning without significant coma.

9-8.2 Specified Aperture Distribution Axisymmetric Dielectric Lens [11]

We use the desired aperture amplitude distribution to specify the relation between the aperture radius r, and the feed angle ψ. Earlier, the Abbe sine condition established this relation. Given a feed power pattern $F(\psi)$ and a required aperture distribution $A(r)$, we relate the two through differential areas:

$$F(\psi) \sin \psi \, d\psi = A(r) r \, dr$$

where an axisymmetrical pattern is assumed. We derive the relation between ψ and r through normalized integrals as in Section 8-20:

$$\frac{\displaystyle\int_0^{\psi} F(\psi) \sin \psi \, d\psi}{\displaystyle\int_0^{\psi_m} F(\psi) \sin \psi \, d\psi} = \frac{\displaystyle\int_0^{r} A(r) r \, dr}{\displaystyle\int_0^{r_m} A(r) r \, dr} \tag{9-47}$$

In any particular design we generate a table, such as Table 8-12, of the feed angle versus its normalized feed pattern integral and the aperture radius versus its normalized aperture distribution integral. For a given feed angle ψ we equate the normalized integrals to compute the corresponding aperture radius. We generate a table of aperture radius versus feed angle, such as Table 8-13, using interpolation techniques. The design is very dependent on feed pattern, because changing the feed pattern alters the table. Low sidelobe aperture distributions require close tolerances and a good specification of the feed pattern.

Once we have the relation between ψ and r, the design follows steps similar to those taken in designing the lens for the Abbe sine condition. We solve the differential

equation (9-43) numerically. We specify the aperture radius by the table generated for the transformation of the feed pattern into the aperture distribution. The requirement for equal path length through the lens determines the axis location z of the outer surface.

$$\begin{aligned} &Ax^2 + Bx + C = 0 \qquad x = z - f \\ &A = n^2 - 1 \\ &B = 2[n^2(f - \rho\cos\psi)] + \rho - K - f \\ &C = [n(\rho\cos\psi - f)]^2 + (r - \rho\sin\psi)^2 - (f + K - \rho)^2 \\ &K = T(n-1) \qquad z = f + \frac{-B + \sqrt{B^2 - 4AC}}{4A} \end{aligned} \tag{9-48}$$

where T is the central thickness and f is the axis focal length.

A successful design requires a number of iterations, starting with different initial conditions. The differential equation solution will diverge to shapes unable to satisfy the equal-path-length side requirement with poor initial conditions. Each design has a narrow range of satisfactory initial conditions. In most cases, increasing the thickness increases the chance for a successful design.

Example A lens was designed to transform the feed pattern of a conical corrugated horn into a circular Taylor distribution with 40-dB sidelobes ($\overline{n} = 8$). The initial conditions were $n = 1.6$, diameter $D = 32$, focal distance $f = 35$, central thickness $T = 9$, and maximum feed angle $\psi_m = 20^\circ$. A table of the feed angle and its normalized power pattern integral, along with the aperture radius and its normalized power distribution integral, was generated. A table of feed angle and the corresponding aperture radius follows from equating normalized integrals. This table is independent of the lens thickness but not the feed pattern.

A Runge–Kutta numerical method is used to solve the differential equation (9-43) subject to the conditions imposed by the aperture radius table and Eq. (9-48) for equal optical path lengths. Figure 9-11 shows a design for a 36° 10-dB beamwidth feed horn (12-dB feed edge taper). The horn dimensions are aperture radius $= 1.90\lambda$ and slant radius $= 9\lambda$ for a maximum quadratic phase deviation $S = 0.2$. A few points of the design are listed in Table 9-9. Other antennas designed with small changes in the feed pattern beamwidth show significant changes in the lens shape near the edges for a constant center thickness. Axisymmetric dielectric lenses can be designed to be independent of frequency because only relative sizes are specified. The lenses tend to be thick to allow room to satisfy the requirement for an equal optical path length.

Zoning lens reduces weight while decreasing bandwidth. Low-sidelobe designs are inherently narrowband, since small changes in the beamwidth of the feed alter the aperture distribution and sidelobe levels. Zoning may not reduce the bandwidth significantly. An antenna designed and tested using the technique above revealed a number of requirements on the design [12]. The sidelobe levels exceeded the design specification for three main reasons. First, the feed pattern was specified as $\sin(\pi U)/\pi U$, an oversimplification of the actual feed pattern. Realistic feed patterns must be used because small changes in the feed pattern require new designs. Second, the surfaces must be matched with quarter-wavelength sections to prevent reflections, unaccounted

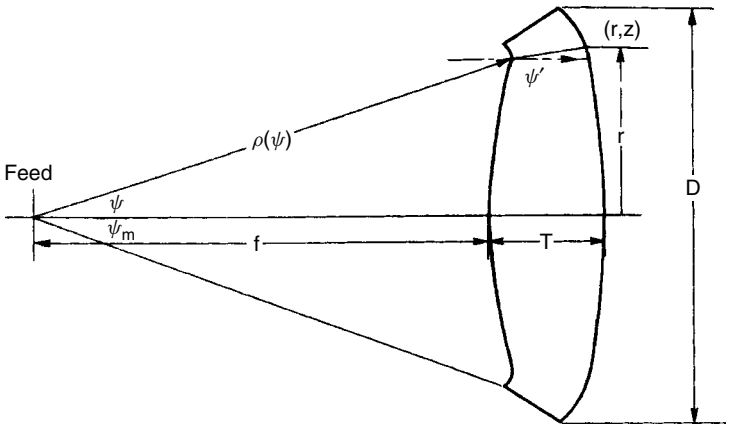

FIGURE 9-11 Dual-surface axisymmetric lens for circular Taylor aperture distribution (40-dB, $\hat{n} = 8$). Lens: $n = 1.6$, $D = 32$, $f = 35$, $T = 9$, $\psi_m = 20°$. Feed: conical corrugated horn, 36° 10-dB beamwidth. $S = 0.2$.

TABLE 9-9 Design of Figure 9-12 for a Specified Aperture Distribution Axisymmetric Dielectric Lens

Feed Angle, ψ (deg)	Inner Surface, $\rho(\psi)$	Horizontal Distance, z	Radius, r	Thickness Along Ray, T
0	35.00	44.00	0	9.00
5	35.31	43.95	3.27	8.78
10	36.14	43.67	6.59	8.08
15	37.69	43.25	10.11	6.86
20	38.71	40.58	16.00	5.03

for in the design, that change the aperture distribution. Third, diffractions from the edges affect the distribution. Increasing the aperture diameter or using a low edge illumination feed reduces these effects.

As designed, the lens exhibits severe coma when scanned by feed lateral offset. Since most lenses are quite thick, zoning can be used to approximate the Abbe sine condition on the inner surface. The lens refracts most of the rays parallel with the axis by the inner surface. If the zones approximate a spherical surface on the average, coma is reduced for the scanned beams. These coma-corrected lenses are useful for multibeam applications when each beam is fed from an offset feed.

9-9 BOOTLACE LENS

The bootlace lens consists of a set of receiving antennas on a surface connected by cables to a set of transmitting antennas on the second surface (Figure 9-12). The cables constrain the path through the lens. We have three degrees of freedom with this lens: (1) input surface, (2) output surface, and (3) cable length. We can change the lens characteristics dynamically by placing phase shifters and/or attenuators in the lines

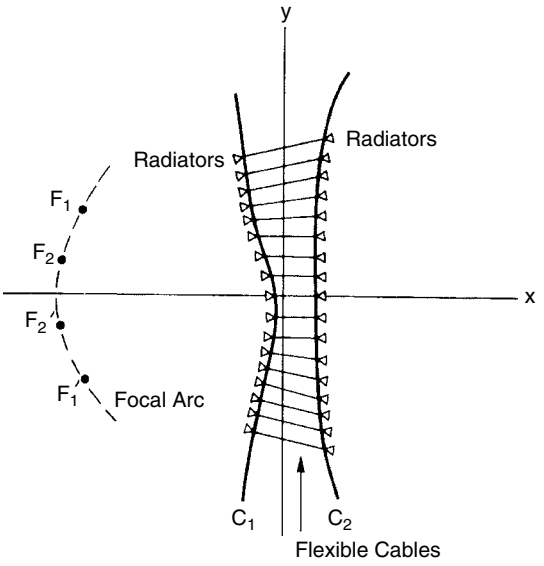

FIGURE 9-12 Bootlace lens. (From [13], Fig. 3, ©1965 IEEE.)

between the input and output radiators and scan one or more beams. The input and output surfaces are arrays, and we can generate multiple beams by placing more than one feed on a focal arc determined by the lens geometry.

The simplest bootlace lens consists of a spherical input surface connected to a plane output surface by equal-length cables. This lens converts spherical waves radiated by the feed into plane waves at the output surface. The lens uses true time delay, which removes bandwidth limitations. Most bootlace lenses are line sources or two-dimensional lenses fed by line sources. The general lens can have four focal points [13] placed symmetrically about the axis of the symmetric structure. The focal arc is chosen on a curve through the focal points to minimize defocusing when feeds are placed off the focal points. A feed at each point along the focal arc produces an output beam in a different direction. Because each feed uses the full aperture, it achieves the full array gain less the loss of projection of the aperture length in the beam direction.

The number of focal points is reduced to three when the lens is further restrained. The Ruze design for a metal plate lens [8] has three focal points, since the waveguides between the surfaces travel in straight lines. There is one central axis focal point and two symmetrically placed focal points. The Rotman [14] lens loses one possible focal point because the output surface is limited to a straight line. A parallel-plate structure in the Rotman lens leads from the possible feed locations to the feed-side surface, which normally is excited by probes in the parallel-plate guide. The lens becomes a feed network that produces multiple beams whose directions depend on the location of the feed on the focal arc. Although perfect focusing is achieved at only three points, the phase error loss associated with points between them is small. Because the Rotman lens feed network is a true time-delay array feed network, we can achieve bandwidths greater than an octave from it.

Rao [15] extends the design of bootlace lenses to three dimensions and shows that the number of focal points cannot be extended beyond four. Because the lens is not

axisymmetric, it has different scanning capabilities in orthogonal planes. Rao designs lenses with two, three, and four focal points on a focal line. Decreasing the number of focal points in one plane increases the scanning capability in the orthogonal plane for a given phase error level.

9-10 LUNEBURG LENS [16, p. 545]

A Luneburg lens, a spherically symmetric lens with a variable index of refraction, radiates a beam in any direction for a feed located opposite the beam. We place the feed phase center either on the surface of the lens or a short distance away. We form multiple beams by feeding the lens at a number of places. Our only restriction is the blockage due to other feeds or support structures. We can rapidly scan a beam by moving a lightweight feed around the sphere or by switching between multiple feeds.

When we place the feed on the outer surface of the sphere, the required index of refraction is

$$n = \sqrt{2 - \left(\frac{r}{a}\right)^2} \tag{9-49}$$

where a is the lens outer radius and r is the inner radius. The dielectric constant n^2 must vary between 2 in the center and 1 on the outer surface. Few feeds have their phase centers on a surface that can be mounted against a sphere. We can move the feed away from the surface by changing the variation of the index of refraction from that given by Eq. (9-49), but the required center index of refraction decreases as we move the feed away from the lens surface. We calculate the variation of the index of refraction from an integral equation, and the curves follow the general shape of Eq. (9-49). For the feed-to-sphere radius of 1.1, the proper center dielectric constant is 1.83 and it varies smoothly to 1 at the lens surface. Similarly, the center dielectric constant starts at 1.68 for the feed-to-sphere radius of 1.2.

The lens changes the amplitude distribution in the aperture compared with the feed. Given the ratio of feed radius to lens radius r_i, the aperture plane power distribution becomes

$$A(r) = \frac{F(\psi)}{r_1^2 \cos \psi} \tag{9-50}$$

where ψ is the feed angle, $F(\psi)$ the feed power pattern, and $A(r)$ the aperture power distribution. Equation (9-50) shows that the lens refracts power toward the edge of the aperture. Lenses have been made by using a series of concentric spherical shells each with a constant dielectric. A minimum of 10 shells is needed for an adequate approximation of the required variation of the dielectric constant.

REFERENCES

1. J. R. Risser, Chapter 11 in S. Silver, ed., *Microwave Antenna Theory and Design*, McGraw-Hill, New York, 1948.
2. S. B. Cohn, Chapter 14 in H. Jasik, ed., *Antenna Engineering Handbook*, McGraw-Hill, New York, 1961.
3. S. Cornbleet, *Microwave Optics*, Academic Press, London, 1976.

4. B. E. A. Saleh and M. C. Teich, *Fundamentals of Photonics*, Wiley, New York, 1991.
5. A. R. Dion, A broadband compound waveguide lens, *IEEE Transactions on Antennas and Propagation*, vol. AP-26, no. 5, September 1978, pp. 751–755.
6. T. Morita and S. B. Cohn, Microwave lens matching by simulated quarter-wave transformers, *IEEE Transactions on Antennas and Propagation*, vol. AP-4, no. 1, January 1956, pp. 33–39.
7. R. W. Kreutel, The hyperboloidal lens with laterally displaced dipole feed, *IEEE Transactions on Antennas and Propagation*, vol. AP-28, no. 4, July 1980, pp. 443–450.
8. J. Ruze, Wide-angle metal-plate optics, *Proceedings of IRE*, vol. 38, no. 1, January 1950, pp. 53–59.
9. J. J. Lee, Numerical methods make lens antennas practical, *Microwaves*, vol. 21, no. 9, September 1982, pp. 81–84.
10. R. Kingslake, *Lens Design Fundamentals*, Academic Press, New York, 1978.
11. J. J. Lee, Dielectric lens shaping and coma-correcting zoning, part I: analysis, *IEEE Transactions on Antennas and Propagation*, vol. AP-31, no. 1, January 1983, pp. 211–216.
12. J. J. Lee and R. L. Carlise, A coma-corrected multibeam shaped lens antenna, part II: experiments, *IEEE Transactions on Antennas and Propagation* vol. AP-31, no. 1, January 1983, pp. 216–220.
13. M. L. Kales and R. M. Brown, Design considerations for two dimensional symmetric bootlace lenses, *IEEE Transactions on Antennas and Propagation*, vol. AP-13, no. 4, July 1965, pp. 521–528.
14. W. Rotman and R. F. Turner, Wide-angle microwave lens for line source applications, *IEEE Transactions on Antennas and Propagation*, vol. AP-11, no. 6, November 1963, pp. 623–632.
15. J. B. L. Rao, Multifocal three-dimensional bootlace lenses, *IEEE Transactions on Antennas and Propagation*, vol. AP-30, no. 6, November 1982, pp. 1050–1056.
16. R. S. Elliott, *Antenna Theory and Design*, Prentice-Hall, Englewood Cliffs, NJ, 1981.